Clinicopathologic features and molecular characteristics of glucose metabolism contributing to ^{18}F-fluorodeoxyglucose uptake in gastrointestinal stromal tumor

Min-Hee Cho

Department of Medical Science

The Graduate School, Yonsei University

Clinicopathologic features and molecular characteristics of glucose metabolism contributing to ^{18}F-fluorodeoxyglucose uptake in gastrointestinal stromal tumor

Directed by Professor Hoguen Kim

The Master's Thesis
submitted to the Department of Medical Science,
the Graduate School of Yonsei University
in partial fulfillment of the requirements for the degree
of Master of Medical Science

Min-Hee Cho

December 2015

This certifies that the Master's Thesis of Min-Hee Cho is approved.

Thesis Supervisor: Hoguen Kim

Thesis Committee Member#1: Kyung-Sup Kim

Thesis Committee Member#2: Jae-Ho Cheong

The Graduate School

Yonsei University

December 2015

ACKNOWLEDGEMENTS

아직도 모르는 것이 너무 많은데 어느덧 졸업을 앞두고 있으니, 기쁘지만 걱정스러운 마음이 더 큽니다. 시행착오 속에서 제가 학위논문을 마무리할 수 있었던 이유는, 학위기간 중 저를 응원해주고 도와주셨던 분들 덕분이라고 생각합니다. 먼저 저를 제자로 받아주시고, 많은 성과를 내지 못했는데 끝까지 기다려주시고 지도해주신 김호근 교수님께 진심으로 감사 드립니다. 더 좋은 학위논문이 될 수 있도록 조언해 주신 김경섭 교수님, 정재호 교수님께도 깊은 감사를 드립니다.

또한 입학할 때 격려해주시고 용기 북돋아 주신 이진아 교수님, 실험을 배워볼 수 있도록 기회를 주셨던 황기철 교수님, 창연오빠, 세연언니 모두 감사 드립니다. 항상 옆에서 응원해줬던 다솜이, 지영이언니, 시정이언니, 복경이, 광현오빠, 용우오빠 너무 고맙고, 다른 실험실이지만 이것저것 많이 알려주고 도움 준 이나언니도 너무 고맙습니다. 그리고 실험하면서 여러 코멘트 해주고 도와준 실험실

선배,후배님들 감사 드립니다.

마지막으로, 몸도 많이 편찮으신데 부족한 딸 여기까지 공부시켜주신 엄마, 아빠 감사하고 사랑한다는 말 전합니다. 제 곁에 있는 것만으로 큰 힘이 됩니다.

졸업은 또 다른 시작이니 새롭게 시작하는 저를 지금처럼 응원해주시고 지켜봐 주시길 바랍니다.

감사합니다.

2015년 12월

저자 조민희 올림

TABLE OF CONTENTS

LIST OF FIGURES

LIST OF TABLES

ABSTRACT

Clinicopathologic features and molecular characteristics of glucose metabolism contributing to ^{18}F-fluorodeoxyglucose uptake in gastrointestinal stromal tumor

Min-Hee Cho

Department of Medical Science

The Graduate School, Yonsei University

(Directed by Professor Hoguen Kim)

Fluorine-18 fluorodeoxyglucose (^{18}F-FDG) positron emission tomography–computed tomography (PET/CT) is useful in the preoperative diagnosis of gastrointestinal stromal tumors (GISTs); however, the molecular characteristics of glucose metabolism of GIST are unknown. We evaluated ^{18}F-FDG uptake on preoperative PET/CT of 40 patients and analyzed the expression of glycolytic enzymes in resected GIST tissues by qRT-PCR, western blotting, and immunohistochemistry. Results of receiver operating

characteristic curve analysis showed that the maximum standardized uptake value (SUVmax) cut-off value of 4.99 had a sensitivity of 89.5%, specificity was 76.2%, and accuracy of 82.5% for identifying tumors with a high risk of malignancy. We found that ^{18}F-FDG uptake correlated positively with tumor risk grade and expression levels of glucose transporter 1 (GLUT1), hexokinase 1 (HK1), and lactate dehydrogenase A (LDHA). Overexpression of GLUT1 and HK1 increased with higher tumor risk grade. In addition, overexpression of glycolytic enzymes M2 isoform of pyruvate kinase (PKM2) and LDHA was observed in GISTs, especially in high-risk tumors. These results indicate increased glycolysis in GISTs and suggest that upregulation of GLUT1, HK1, PKM2, and LDHA may play an important role in GIST tumorigenesis and may be useful in the preoperative prediction of malignant potential.

Key words: gastrointestinal stromal tumors, ^{18}F-FDG uptake, glucose metabolism, malignancy

Clinicopathologic features and molecular characteristics of glucose metabolism contributing to ^{18}F-fluorodeoxyglucose uptake in gastrointestinal stromal tumor

Min-Hee Cho

Department of Medical Science

The Graduate School, Yonsei University

(Directed by Professor Hoguen Kim)

I. INTRODUCTION

Gastrointestinal stromal tumors (GISTs), the most common non-epithelial neoplasms of the gastrointestinal (GI) tract, are defined as "*KIT* or *PDGFRA* mutation-driven mesenchymal tumors that can occur anywhere in the GI tract".[1] Preoperative diagnosis of GISTs and assessment of their malignant potential are difficult because most GISTs are located in the submucosa. Tumor grading is therefore based primarily on mitotic index and tumor diameter.

The clinical usefulness of ^{18}F-fluorodeoxyglucose (FDG) positron emission tomography–computed tomography (PET/CT) has been demonstrated in tumor staging, treatment response assessment, and prognosis prediction in various tumors.[2-6] This technique is also used in tumor staging and evaluation of targeted therapy response in GISTs.[7-12]

Many tumors depend on aerobic glycolysis for rapid growth beyond that supported by the vasculature. ^{18}F-FDG is an analogue of glucose that allows noninvasive evaluation of the tumor's glucose metabolism, which can predict treatment response and patient prognosis. ^{18}F-FDG enters the cell through glucose transporters (GLUT), is phosphorylated to ^{18}F-FDG-6-PO_4 by hexokinase (HK), and is then "trapped" in the cell as it is not further metabolized, allowing PET/CT acquisition 1 hour after ^{18}F-FDG injection. Upregulation of GLUT and HK expression is associated with increased glucose metabolism and ^{18}F-FDG uptake in tumors. For example, previous studies have shown that increased GLUT1 expression correlates with higher ^{18}F-FDG uptake in lung and breast carcinomas.[13-15]

Although ^{18}F-FDG PET/CT is useful for the preoperative diagnosis of GISTs, the detailed molecular mechanisms underlying glucose metabolism in these tumors and specific characteristics associated with tumor risk grade are not well

understood. Tumor cells consume large amounts of glucose and produce large amounts of lactate compared to normal cells, even in the presence of oxygen. This metabolic switch from oxidative phosphorylation to increased glycolysis (i.e., the Warburg effect) is a common characteristic of malignant tumors[16,17] and regulated by transcription factors, such as hypoxia inducible factor-1α (HIF-1α), v-myc avian myelocytomatosis viral oncogene homolog (c-Myc), and tumor suppressor p53 (p53).[18-20] In gastric cancer, ^{18}F-FDG accumulation represents tissue hypoxia, rather than GLUT expression.[21] However, analysis of the enzymes involved in glycolysis has not been performed in GISTs, and it is unclear whether the Warburg effect occurs in GISTs. Qualitative and quantitative analysis of glycolytic enzyme expression and their relationship with GIST tumor risk grade may clarify whether the Warburg effect occurs in GISTs. In this study, we aimed to identify 1) the relationship between maximum standardized uptake value (SUVmax) on preoperative ^{18}F-FDG PET/CT with GLUT and HK expression in GISTs, 2) the specific isoforms of GLUT and HK that are upregulated according to GIST tumor risk grade, and 3) alterations in the expression of various glycolytic enzymes according to tumor risk grade.

By performing this study, we expect to identify the molecular biomarkers predictive of malignant GISTs that can be used in preoperative biopsy or

cytology specimens and the molecular mechanisms of GIST detection by ^{18}F-FDG PET/CT.

II. MATERIALS AND METHODS

1. Patient selection

Our patient selection criteria specified the inclusion of patients diagnosed with GIST who underwent surgery after preoperative ^{18}F-FDG PET/CT, and a total of 40 GIST patients were included in our study. The cases were identified prospectively and consecutively between 2003 and 2013 at Severance Hospital, Yonsei University College of Medicine and from the Liver Cancer Specimen Bank, National Research Resource Bank Program of the Korea Science and Engineering Foundation of the Ministry of Science and Technology. Written informed consent for use of GIST tissues was obtained from all patients, and use of these tissues for research purposes was approved by the Institutional Review Board of Yonsei University of College of Medicine. Risk of malignancy was categorized according to the system described by Fletcher et al.[22]

2. Mutational analysis

DNA extraction was performed by using the QIAamp DNA FFPE Tissue Kit (Qiagen, GmbH, Hilden, Germany) according to the manufacturer's instructions. The Primers used to amplify v-kit Hardy-Zuckerman 4 feline sarcoma viral

oncogene homolog (*KIT*) exons are EXON9, 5'-AGT ATG CCA CAT CCC AAG TG-3' (forward) and 5'-TGA CTG ATA TGG TAG ACA GAG CC-3' (reverse); EXON11, 5'-GGC ATG ATG TGC ATT ATT GTG-3' (forward) and 5'-TGG CAA ACC TAT CAA AAG GG-3' (reverse); EXON13, 5'-ATG CGC TTG ACA TCA GTT TG-3' (forward) and 5'-AAG CAG TTT ATA ATC TAG CAT TGC C-3' (reverse); and EXON17, 5'-TGT GAA CAT CAT TCA AGG CG-3' (forward) and 5'-AAA TGT GTG ATA TCC CTA GAC AGG-3' (reverse). PCR was carried out using a Veriti thermal cycler (Life Technologies, USA) with the following amplification conditions: 35 cycles of denaturation at 94°C for 30 sec, annealing at 60°C for 30 sec, and extension at 72°C for 1 min. The amplified products were purified using Agencourt AMPure XP (Beckman Coulter Genomics, Danvers, MA), and direct sequencing was performed using the BigDye Terminator Ready Reaction Cycle Sequencing kit and an ABI Prism 3130 genetic analyzer (Life Technologies).

3. PET/CT protocol and quantification

All patients underwent routine ^{18}F-FDG PET/CT scans with either the DSTe PET/CT scanner (GE Healthcare, Milwaukee, WI) or the Biograph TruePoint 40 PET/CT scanner (Siemens Medical Systems, CTI, Knoxv/ille, TN). Before

^{18}F-FDG injections, all patients fasted for at least 6 hr, and peripheral blood glucose levels were confirmed to be ≥140 mg/dL. The ^{18}F-FDG dose of approximately 5.5 MBq/kg body weight was administered intravenously 1 hour before image acquisition. After the initial low-dose CT (DSTe: 30mA, 130 kVp, Biograph TruePoint: 36 mA, 120 kVp), standard PET imaging was performed from neck to the proximal thighs (acquisition time, 3 min/bed) in three-dimensional mode. Images were then reconstructed using ordered-subset expectation maximization (2 iterations, 20 subsets).

Images were reviewed by an experienced nuclear medicine specialist on a GE AW 4.0 workstation. On PET scans, a volume of interest (VOI) was drawn on the primary lesion; SUVmax of the GIST was recorded.

4. Immunohistochemistry

Formalin-fixed and paraffin-embedded GIST tissue specimens were cut into 4-μm thick sections, and immunohistochemistry (IHC) analysis was performed using the Ventana Discovery XT autoimmunostainer (Ventana, Tucson, AZ) with antibodies against GLUT1 (1:100; Millipore, Temecula, CA), HK1 (1:800; Cell Signaling Technology, Beverly, MA), PKM2 (1:500; Cell Signaling Technology), and LDHA (1:100; Cell Signaling Technology). IHC results were

scored based on staining intensity as follows: 0, no staining; 1, weak staining (faint protein expression in tumor cells or definite expression in <30% of tumor cells); or 2, strong staining (definite protein expression in >30% of tumor cells).

5. Western blotting

Whole lysates from GIST tissues were prepared using passive lysis buffer (Promega, Madison, WI) with a protease inhibitor cocktail (Roche, Mannheim, Germany). Total protein lysates (50μg) were loaded into each lane, size-fractionated by SDS-PAGE and transferred to a nitrocellulose membrane that was blocked with Tris-buffered saline-Tween 20 containing 5% skim milk. Primary antibodies against GLUT1 (1:500; Millipore), HK1 (1:1,000; Cell Signaling Technology), PKM2 (1:1,000; Cell Signaling Technology), LDHA (1:1,000; Cell Signaling Technology), β-actin (1:2,000; Cell Signaling Technology), and glyceraldehyde 3-phosphate dehydrogenase (GAPDH, 1:100,000; Trevigen, Gaitherburg, MD) were incubated with the membrane for overnight at 4℃. After washing, membranes were incubated with goat anti-rabbit or mouse IgG-HRP conjugated secondary antibody (Santa Cruz Biotechnology, Santa Cruz, CA), washed, and then developed using western blotting luminol reagent (Santa Cruz Biotechnology). Protein band intensity

was analyzed by using a LAS-4000 Mini camera (Fujifilm, Tokyo, Japan).

6. Quantitative reverse transcription-polymerase chain reaction

Quantitative reverse transcription-polymerase chain reaction (qRT-PCR) analysis was carried out in a final reaction volume of 20 μl with Premix Ex Taq II (Takara Bio, Otsu, Japan) according to the manufacturer's protocol. All reactions were run in triplicate on the StepOnePlus Real-Time PCR System (Applied Biosystems, Foster City, CA). Primer sequences are as follows: Beta-actin, 5'-GGA CCT GAC TGA CTA CCT CAT-3' (forward) and 5'-CGT AGC ACA GCT TCT CCT TAA T-3' (reverse); GLUT1, 5'-CTC CTG CCC TGT TGT GTA TAG-3' (forward) and 5'-CAG GAG TGA GGT GGT GTA TTT-3' (reverse); GLUT2, 5'-CTA AAG GGC AGG TGG TTC TAA T-3' (forward) and 5'-TTG CAT CCT CAG GTT TCT AGT T-3' (reverse); GLUT3, 5'-GCT GGG CAT CGT TGT TGG A-3' (forward) and 5'-GCA CTT TGT AGG ATA GCA GGA AG-3' (reverse); GLUT4, 5'-GGC TTC TTC ATC TTC ACC TTC T-3' (forward) and 5'-GGT TTC ACC TCC TGC TCT AAA-3' (reverse); HK1, 5'-CAC ATT GAT CTG GTG GAA GGA-3' (forward) and 5'-CTC TGT CCG GAT GTC TTC TAA TG-3' (reverse); HK2, 5'-AGC CAC CAC TCA CCC TAC TGC-3' (forward) and 5'-CTG GAG CCC ATT GTC

CGT TAC-3' (reverse); PKM2, 5′-ATT ATT TGA GGA ACT CCG CCG CCT-3′ (forward) and 5′-ATT CCG GGT CAC AGC AAT GAT GG-3′ (reverse); LDHA, 5'-ACC CAG ATT TAG GGA CTG ATA AAG-3' (forward) and 5'-CCA ATA GCC CAG GAT GTG TAG-3' (reverse).

7. Hexokinase and lactate dehydrogenase activity assay

Hexokinase (HK) and lactate dehydrogenase (LDH) activities in GIST tissues were determined using a colorimetric (450 nm) kit (Sigma-Aldrich, St Louis, MO) according to the manufacturer's recommended protocol. Each sample was diluted as necessary to fall in the linear range of the standard curve and assayed in duplicate. Briefly, 10 μl samples were mixed with assay buffer in HK activity assay and 5 μl samples were mixed with assay buffer in LDH activity assay. Absorbance was measured at room temperature every 5 min (HK activity) and at 37°C every 2-3 min (LDH activity). Both enzyme activities were assessed using the following equation: $B \times$ sample dilution factor/$(T_{final} - T_{initial}) \times V$; where B is the amount of NADH generated between $T_{initial}$ and T_{final}, and $(T_{final} - T_{initial})$ indicates the reaction time. V is the sample volume (mL) added to the reaction well.

8. Statistical analysis

Relationships between tumor risk grade and other parameters were evaluated using either chi-square test or one-way analysis of variance. Correlation analysis was performed with Pearson's or Spearman's correlation test. Student's *t*-test was used to compare two groups of continuous variables. The area under the receiver operating characteristic (ROC) curve was used to determine the SUV cut-off level able to predict tumor risk grade with the highest sensitivity. Data are expressed as mean ± standard deviation (SD); $P<.05$ was considered significant. Statistical analysis was performed using SPSS for Windows (version 21.0; SPSS Inc., USA).

III. RESULTS

1. Clinicopathologic characteristics and ^{18}F-FDG uptake of 40 GISTs

Of the 40 patients included in the study, 22 were women and 18 were men , and mean patient age was 59 yr (range 20–83) (Table 1). Of the 40 GIST lesions, 18 were located in the stomach, 22 were located in the small or large intestine.

Five lesions were not well visualized on PET (SUVmax<2.5), 12 showed moderate FDG uptake (2.5<SUVmax<5.0), and 23 showed intense FDG uptake (SUVmax≥5.0). High-risk tumors were more common in men (Table 2). FDG uptake did not differ significantly between gastric GISTs and non-gastric GISTs (data not shown). Histologic features of representative cases are shown in Figure 1A.

KIT mutations were found in 32 cases (32/40, 80%). No mutations of *KIT* gene were found in the remaining 8 cases. Among the 32 mutations in *KIT*, a deletion was found in 19 cases (19/32, 59.4%), point mutations in 9 (9/32, 28.1%), and insertion in 4 (4/32, 12.5%) (Table 1). Relationships between mutation status of *KIT* and clinicopathologic parameters were analyzed and listed on Table 3.

Table 1. Demographic and clinicopathologic features of 40 patients with GISTs

			Tumor		Mutation status
No.	**Age**	**Sex**	**Site**	**SUVmax**	***KIT***
1	66	Male	Stomach	5.7	K550_V555 del
2	46	Female	Jejunum	4.5	M552_D572 del
3	71	Male	Stomach	5.2	V559D
4	67	Male	Stomach	12.4	M552_Y553 del
5	65	Female	Ileum	16.9	Y503_F504 ins AY
6	58	Male	Stomach	12.5	K558_E562 del
7	65	Female	Jejunum	19.2	M552_I571 del
8	53	Male	Stomach	8.9	W557_K558 del
9	56	Male	Jejunum	9.2	wild
10	77	Male	Ileum	14.7	Y503_F504 ins AY
11	54	Male	Stomach	12.0	V559D
12	71	Male	Stomach	21.4	Q556_K558 del
13	58	Female	Rectum	8	wild
14	49	Male	Jejunum	5.4	Y568_L576 del
15	66	Male	Stomach	14.5	W557_K558 del
16	27	Male	Jejunum	14.2	W557_V560 del
17	60	Female	Stomach	3.2	D579 del
18	35	Female	Ileum	6.7	Q556_V560 del
19	65	Female	Stomach	13	wild
20	69	Female	Stomach	8.1	K558_I563 del
21	22	Female	Stomach	5.0	T574_K581 del
22	73	Female	Stomach	4.9	W557R
23	83	Female	Stomach	2.4	wild

24	67	Female	Duodenum	9.5	Y503_F504 ins AY
25	75	Male	Jejunum	2.9	wild
26	49	Female	Stomach	2.9	wild
27	54	Female	Duodenum	7.9	W557_K558 del
28	64	Female	Ileum	10.1	Y503_F504 ins AY
29	53	Female	Jejunum	2	wild
30	20	Female	Duodenum	3.9	W557_K558 del
31	58	Male	Jejunum	2.2	V560 del
32	69	Male	Jejunum	4.8	wild
33	52	Female	Duodenum	4.3	V560D
34	75	Male	Duodenum	2.9	V559D
35	59	Male	Duodenum	1.8	D572Y
36	57	Female	Stomach	2.6	L576P
37	62	Female	Stomach	3.7	L576P
38	65	Female	Duodenum	2.6	W557_K558 del
39	64	Male	Stomach	2.4	V560D
40	49	Female	Jejunum	12.2	W557_K558 del

Table 2. Relationships between GIST risk grade and ^{18}F-FDG uptake and demographic and clinicopathologic factors

	Low (n=13)	Intermediate (n=8)	High (n=19)	*P* value
Age, years	57.5±13.3	61.5±19.4	58.4±12.5	0.814
Gender, n				
Male	5	1	12	0.046*
Female	8	7	7	
Tumor size, cm	3.2±1.0	5.9±2.1	9.6±4.0	<.001*
Mitotic count, /50 HPF	2.1±1.3	4.9±3.5	27.5±35.2	0.013*
SUVmax	4.3±3.2	5.4±2.7	10.9±5.2	<.001*

**P* value was calculated either by chi-square test or one-way analysis of variance

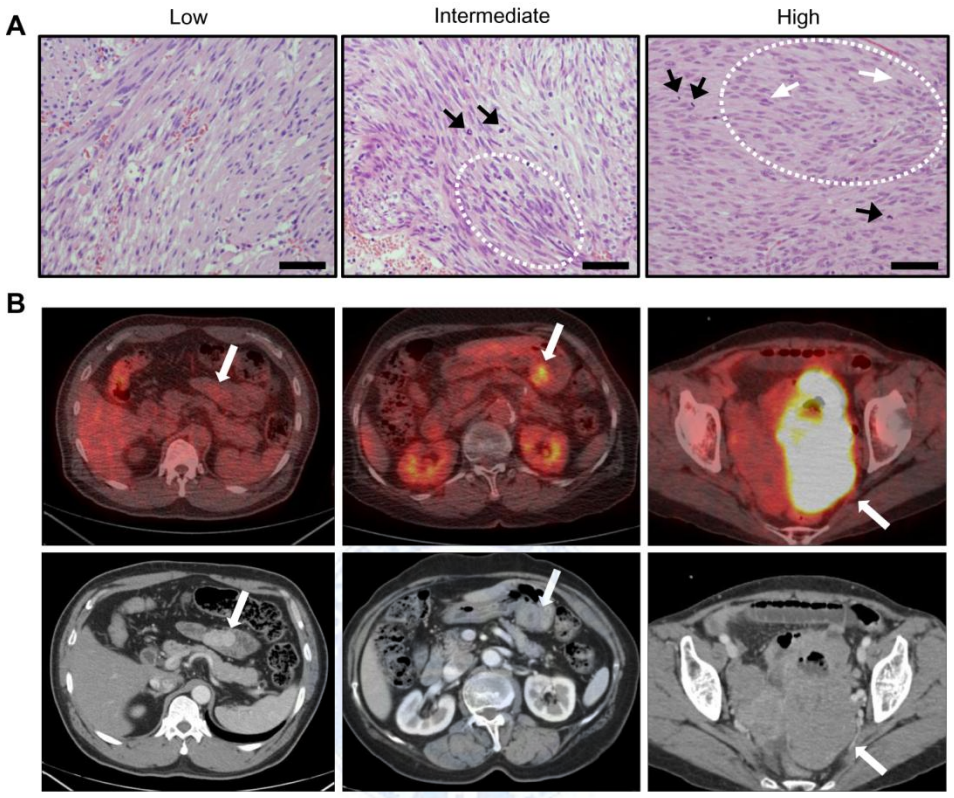

Figure 1. **Histologic features of GISTs and Representative cases showing ^{18}F-FDG uptake intensity according to tumor risk grade.** (A) Low-risk GIST showing proliferation of bland-looking spindle cells with infrequent mitoses (1/50 HPFs) (left panel). Intermediate-risk GIST showing mild nuclear pleomorphism (dashed line) with occasional mitosis (10/50 HPFs; black arrows) (middle panel). High-risk GIST showing proliferation of spindle cells with hyperchromatic nuclei (white arrows), moderate pleomorphism, and frequent mitoses (13/50 HPFs) (right panel). Scale bar, 100μm; ×200. (B) Low-risk

GIST: 58-year-old man with mild ^{18}F-FDG uptake (SUVmax=2.2) in the proximal jejunum (left panel). Intermediate-risk GIST: 73-year-old woman with moderate ^{18}F-FDG uptake (SUVmax=4.9) (middle panel). High-risk GIST: 65-year-old woman with intense ^{18}F-FDG uptake (SUVmax=19.2) (right panel).

Table 3. Comparison of clinicopathologic categories between GISTs with *KIT* mutation

	Mutation status of *KIT*			
Category	Wild (n=8)	Exon 11 (n=28)	Exon 9 (n=4)	*P* value
Age, years	63.5±11.7	56.0±14.7	68.3±6.0	0.146
Gender, n				
Male	3	14	1	0.574
Female	5	14	3	
Tumor size, cm	7.6±4.2	6.6±4.3	6.3±2.2	0.818
Mitotic count, /50 HPF	19.8±28.4	14.0±28.7	9.8±7.6	0.812
Tumor site, n				
stomach	3	15	0	0.117
non-stomach	5	13	4	
Tumor grade				
Low	2	10	1	0.692
Intermediate	3	4	1	
High	3	14	2	
GLUT1				
Negative	1	3	0	0.126
Positive	6	20	1	
Strong	1	5	3	
HK1				

Negative	1	4	0	0.124
Positive	6	19	1	
Strong	1	5	3	
PKM2				
Negative	2	5	1	0.966
Positive	5	18	2	
Strong	1	5	1	
LDHA				
Negative	0	0	0	0.162
Positive	4	14	0	
Strong	4	14	4	
SUVmax	5.6±4.0	7.5±5.3	12.8±3.6	0.074

2. Correlation between ^{18}F-FDG uptake and tumor risk grade

Tumor risk grade [22] correlated significantly with ^{18}F-FDG uptake (P<.001) (Table 2 and Figure 1B). SUVmax was lower for low-risk (4.3±3.2) and intermediate-risk tumors (5.4±2.7) than for high-risk tumors (10.9±5.2; P<.001).

To evaluate the usefulness of ^{18}F-FDG PET/CT in predicting the malignant potential of GISTs, we compared high-risk tumors with intermediate- and low-risk tumors. ROC curve analysis showed that a SUVmax cut-off of 4.99 was the most sensitive for predicting malignancy, and area under curve was 0.875 (P<.001). Using this SUVmax cut-off value to differentiate high-risk tumors from low- and intermediate-risk tumors, sensitivity was 89.5% (16/18), specificity was 76.2% (17/22), and accuracy was 82.5% (32/40).

3. Overexpression of GLUT1 and HK1 in GISTs according to tumor risk grade

Because isoforms of GLUT and HK are overexpressed in tumors and associated with ^{18}F-FDG uptake, we evaluated the expression of four isoforms of GLUT (GLUT 1, 2, 3, and 4) and two isoforms of HK (HK1 and HK2) in the 40 GISTs. First, we analyzed total HK activity. We found that HK activity was

significantly upregulated in high-risk GISTs, compared to low-risk and intermediate-risk GISTs (P<.05) (Figure 2). Results of qRT-PCR analysis showed gradual increases in GLUT1 and HK1 expression with higher tumor risk grade (Figure 3). In contrast, expression of *GLUT 2, 3, 4,* and *HK2* was not correlated with tumor risk grade at the mRNA level. Expression of *GLUT1* was significantly increased in high-risk GISTs (1.3±1.32) compared to low-risk GISTs (0.27±0.32; *P*<.01). Similarly, *HK1* expression was increased in intermediate-risk (1.65±0.48) and high-risk GISTs (1.58±1.10) compared to low-risk GISTs (0.94±0.68; *P*<.05).

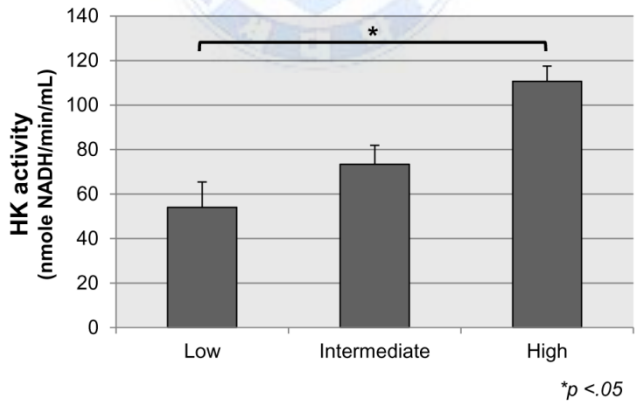

Figure 2. Total HK activity in GISTs. Elevated HK activity is found in high-grade GISTs. Results are expressed as mean±SD of three independent experiments. **P*<.05 based on the Student's *t*-test.

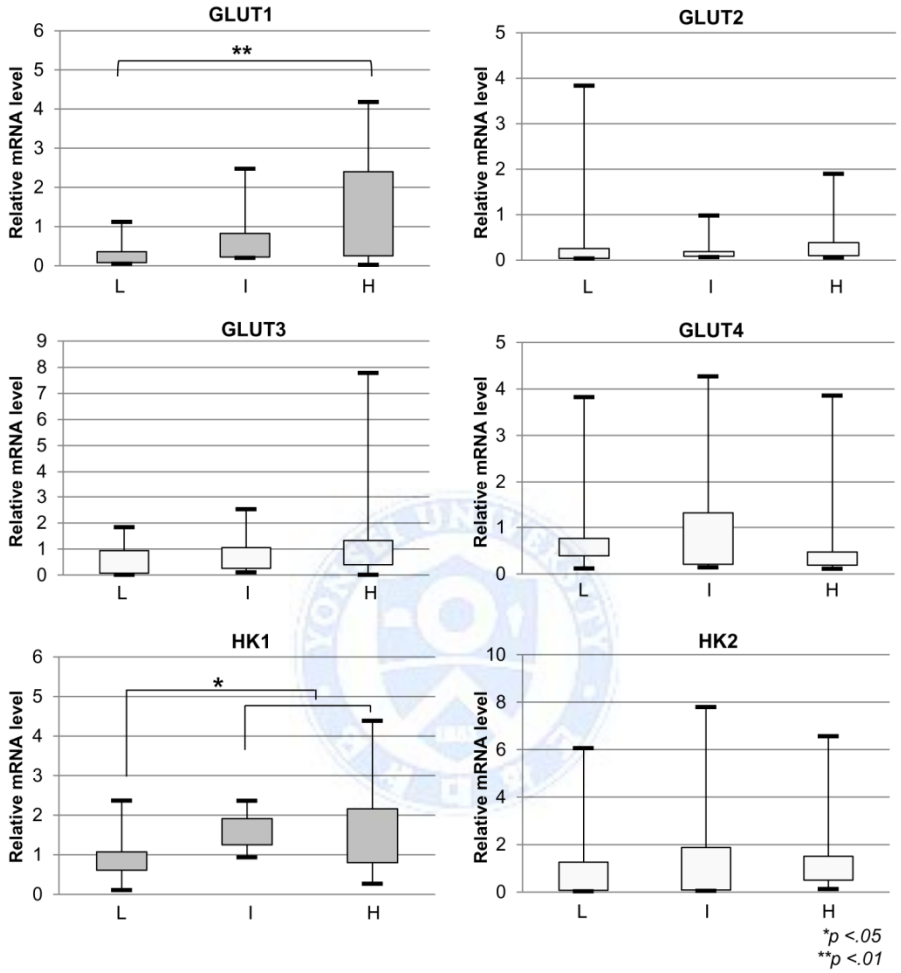

Figure 3. GLUTs (GLUT1, 2, 3, and 4) and HKs (HK1 and 2) expression according to GIST risk grade, as assessed by quantitative RT-PCR. GLUT1 and HK1 mRNA levels increased with higher tumor risk grade. L=low risk; I=intermediate risk; H=high risk. **P*<.05; ***P*<.01 based on the Student's *t*-test.

We next analyzed GLUT1 and HK1 protein expression by IHC and western blot analysis. GLUT1 and HK1 protein were detected in most GISTs; however, GLUT1 was not detected in four GISTs, and HK1 was not detected in five GISTs (Table 4). Most of the tumors lacking expression of these two proteins were low-risk GISTs (Table 4 and Figure 4A). Results of IHC staining showed that SUVmax correlated with both GLUT1 expression (r_s=0.465, P=0.002) and HK1 expression (r_s=0.446, P=0.004) (Figure 4B). GLUT1 and HK1 expression were not affected by tumor size and mitotic count (Table 5). These findings suggest that GLUT1 and HK1 expression are related to PET signals. Results of western blotting analysis showed expression patterns of GLUT1 and HK1 that were similar to qRT-PCR and IHC results (Figure 4C).

Table 4. Relationships between GLUT1 and HK1 immunohistochemical expression and GIST risk grade

Category	Low (n=13)	Intermediate (n=8)	High (n=19)	*P* value
GLUT1, n (%)				
Negative	3 (23.1)	0 (0.0)	1 (5.3)	0.024*
Positive	10 (76.9)	7 (87.5)	10 (52.6)	
Strong	0 (0.0)	1 (12.5)	8 (42.1)	
HK1, n (%)				
Negative	4 (30.8)	0 (0.0)	1 (5.3)	0.036*
Positive	9 (69.2)	6 (75.0)	11 (57.9)	
Strong	0 (0.0)	2 (25.0)	7 (36.8)	

**P* value was calculated either by chi-square test or Fisher's exact test.

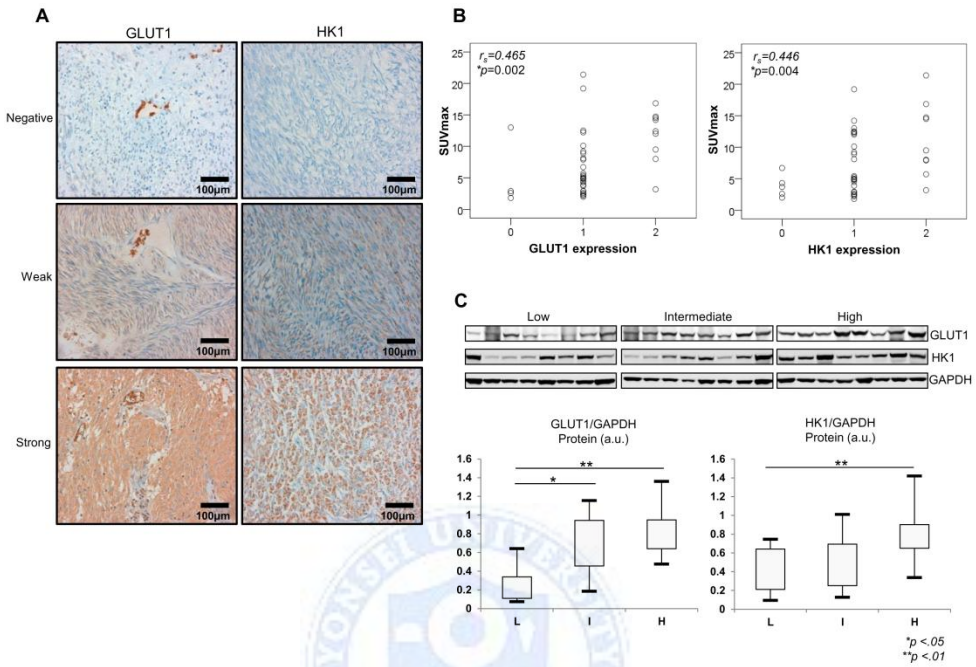

Figure 4. SUVmax correlated with GLUT1 and HK1 expression. (A) Immunohistochemical analysis of GLUT1 and HK1 expression in representative tumor tissues (×200). (B) Correlation between ^{18}F-FDG uptake and GLUT1 and HK1 expression (r_s=Spearman's correlation coefficient). (C) Western blotting and densitometric analysis of GLUT1 and HK1 expression in representative tissues. The densitometric data are normalized to GAPDH and shown as arbitrary units. L=low risk; I=intermediate risk; H=high risk. **P*<.05; ***P*<.01 based on the Student's *t*-test.

Table 5. Relationships between GLUT1 and HK1 immunohistochemical expression and tumor size and mitotic count

	GLUT1 expression			
	Negative (n=4)	**Positive (n=27)**	**Strong (n=9)**	***P* value**
Tumor size, cm	6.6±6.9	6.2±4.0	8.4±2.6	0.386
Mitotic count, /50 HPF	19.0±34.0	12.1±28.5	20.7±19.7	0.682
	HK1 expression			
	Negative (n=5)	**Positive (n=26)**	**Strong (n=9)**	***P* value**
Tumor size, cm	4.2±2.4	6.5±3.8	8.9±4.8	0.106
Mitotic count, /50 HPF	31.6±67.3	9.4±13.5	20.6±19.9	0.186

4. Enhanced expression of PKM2 and LDHA in high-risk GISTs

In order to elucidate the presence of the Warburg effect in GISTs, we evaluated mRNA and protein expression levels for PKM2 and LDHA. Results of qRT-PCR showed a gradual increase in PKM2 and LDHA expression with higher tumor risk grade (Figure 5). *PKM2* expression was significantly higher in high-risk GISTs (3.39±3.51) than in low-risk (0.69±0.67) and intermediate-risk GISTs (0.85±0.36; $P<.05$). Similarly, *LDHA* expression was significantly higher in high-risk GISTs (1.37±1.09) than in low-risk (0.49±0.63) and intermediate-risk GISTs (0.89±0.92; $P<.05$).

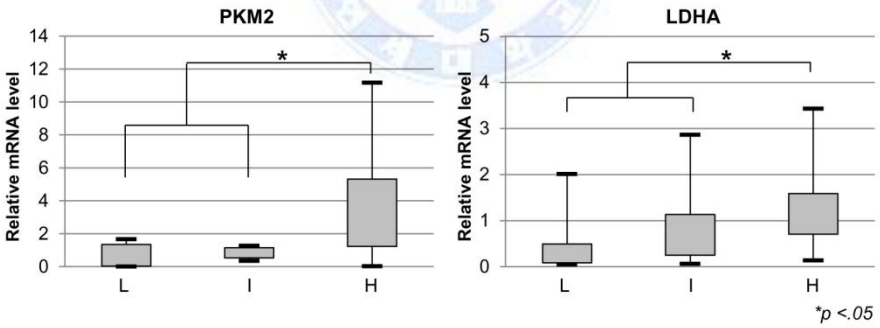

Figure 5. PKM2 and LDHA expression according to GIST risk grade, as assessed by quantitative RT-PCR. PKM2 and LDHA mRNA levels increased with higher tumor risk grade. L=low risk; I=intermediate risk; H=high risk. *$P<.05$ based on the Student's *t*-test.

Next, we evaluated protein levels of PKM2 and LDHA in the 40 GISTs by IHC and western blotting analysis. These two glycolytic enzymes were detected in most GISTs; however, PKM2 was not expressed in eight GISTs (Table 6). Most of the tumors lacking protein expression of these enzymes were low-risk GISTs. Protein levels of PKM2 and LDHA were increased in intermediate- and high-risk GISTs (Table 6 and Figure 6A). We also found a positive correlation between SUVmax and LDHA protein expression. SUVmax was significantly higher in tumors with strong LDHA expression than in tumors with weak LDHA expression (r_s=0.466, P=0.002) (Figure 6B). Results of western blotting analysis showed that PKM2 and LDHA expression patterns were similar to IHC results (Figure 6C). Additionally, we measured LDH activity in our GIST tissues to evaluate metabolism status. LDH activity was significantly upregulated in high-risk GISTs, compared to low-risk and intermediate-risk GISTs (P<.01) (Figure 7). These findings suggest that upregulation of LDHA is involved in the malignant potential and PET signal of GISTs.

Table 6. Relationships between PKM2 and LDHA immunohistochemical expression and GIST risk grade

Category	Low (n=13)	Intermediate (n=8)	High (n=19)	*P* value
PKM2, n (%)				
Negative	6 (46.2)	1 (12.5)	1 (5.3)	0.02*
Positive	7 (53.8)	6 (75.0)	12 (63.2)	
Strong	0 (0.0)	1 (12.5)	6 (31.6)	
LDHA, n (%)				
Negative	0 (0.0)	0 (0.0)	0 (0.0)	0.016*
Positive	10 (76.9)	3 (37.5)	5 (26.3)	
Strong	3 (23.1)	5 (62.5)	14 (73.7)	

**P* value was calculated either by chi-square test or Fisher's exact test.

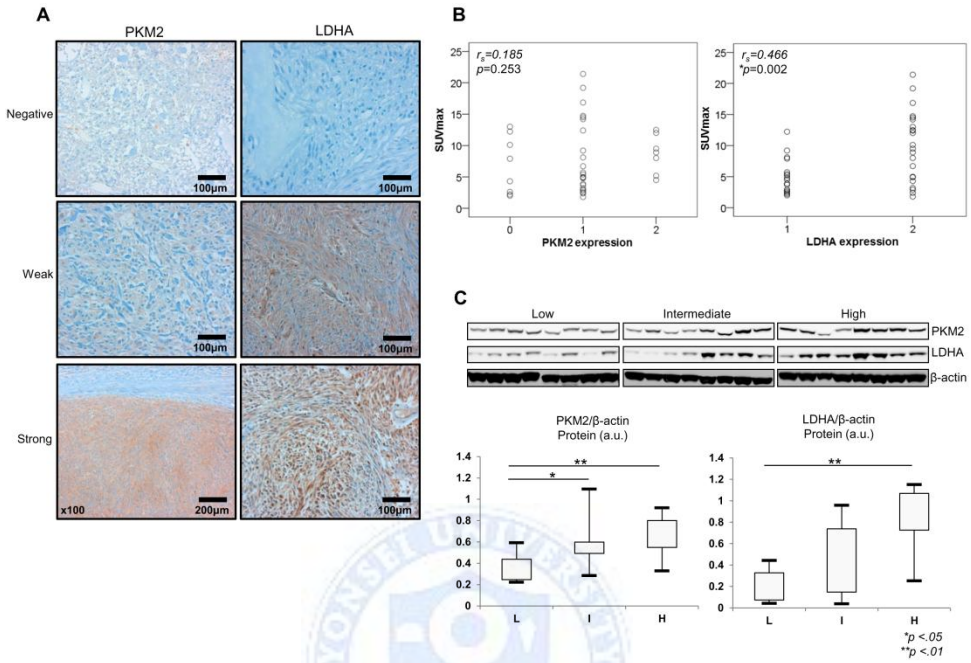

Figure 6. SUVmax correlated with LDHA expression. (A) Immunohistochemical analysis of PKM2 and LDHA expression in representative tumor tissues. (B) Correlation between ^{18}F-FDG uptake and PKM2 and LDHA protein expression (r_s=Spearman's correlation coefficient). (C) Western blotting and densitometric analysis of PKM2 and LDHA expression in representative tissues. The densitometric data are normalized to β-actin and shown as arbitrary units. **P*<.05; ***P*<.01 based on the Student's *t*-test.

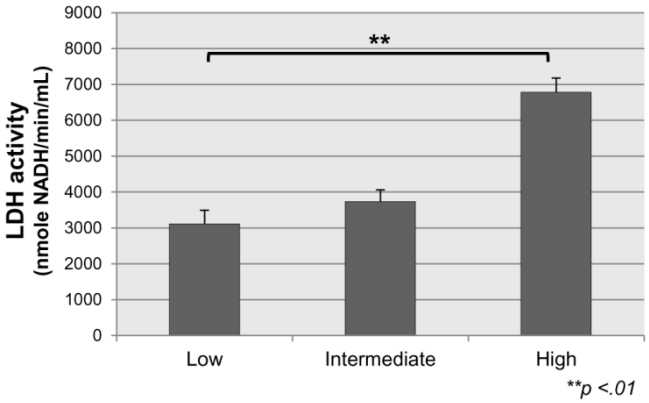

Figure 7. LDH activity in GISTs. Elevated LDH activity is found in high-grade GISTs. Results are expressed as mean±SD of three independent experiments. ***P*<.01 based on the Student's *t*-test.

IV. DISCUSSIONS

In this study, we evaluated clinicopathologic factors contributing to ^{18}F-FDG uptake in the GISTs of 40 consecutive patients. Positive correlations were found between ^{18}F-FDG uptake and several clinicopathologic features and metabolic factors. SUVmax correlated with expression of GLUT1, HK1, and LDHA; and NIH risk group. The optimal SUVmax cut-off value for identifying tumors with a high risk of malignancy (NIH risk classification) was 4.99 (sensitivity, 89.5%; specificity, 76.2%). These findings suggest that PET/CT may be useful for preoperative assessment of malignant potential.

We demonstrated significant overexpression of GLUT1 and HK1 protein in high-risk GISTs by IHC and western blot analysis. We also demonstrated that HK activity in upregulated in high-risk GISTs. GLUT and HK are important for glucose uptake, and the GLUT family of transporters has been implicated in ^{18}F-FDG uptake, with GLUT1 and GLUT3 in particular playing important roles in ^{18}F-FDG accumulation.[13,23] The role of HK in ^{18}F-FDG uptake has been studied in various tumors.[15,24,25] In our study, the isoforms GLUT1 and HK1 were specifically overexpressed in high-risk GISTs, however, the expression levels of GLUT2, 3, 4, and HK2 showed no relationship with GIST risk grade. Overexpression of GLUT1 in the cell membrane had been reported in many

tumors, and overexpression of GLUT2 and GLUT3 has been reported in hepatocellular carcinoma and malignant lymphoma, respectively.[26,27] Although GLUT1, as well as GLUT3 and GLUT4, expression was found in one GIST cell line (GIST-T1),[28] only the expression of GLUT1 was related to GIST risk grade. The paired overexpression of GLUT1 and HK1 in GISTs, and the correlation between increased overexpression of these two proteins and tumor risk grade provide evidence for increased glucose uptake and abnormal glucose metabolism in GISTs, which may be useful in preoperative diagnosis and the development of novel therapeutic targets.

In this study, we demonstrated that the Warburg effect exists in GISTs and observed a correlation between ^{18}F-FDG uptake and tumor risk grade. Most GISTs evaluated in this study showed significant overexpression of the glycolytic enzymes PKM2 and LDHA, with the degree of overexpression increasing with higher tumor risk grade. This metabolic switch from oxidative phosphorylation to increased glycolysis is one of the principle biochemical characteristics of malignant cells.[16] In addition, PKM2 possesses protein tyrosine kinase activity and plays a role in modulating gene expression, thereby contributing to tumorigenesis.[29] For example, enhanced PKM2 expression correlates with aggressive tumor behavior (in vivo tumor growth, tumor cell

proliferation, migration) in colon cancer.[30] LDHA expression is also elevated in many types of cancers and is linked to tumor growth, maintenance, and invasion.[31-34] Therefore, LDHA inhibition may restrict the energy supply in cancer cells, thereby decreasing their tumorigenicity.[24,35] This enzyme may also be useful as a diagnostic marker or predictive biomarker for many types of cancer, as well as a therapeutic target for new anti-cancer treatments. In addition, the correlation between ^{18}F-FDG accumulation and LDHA expression and the possible modulation of ^{18}F-FDG uptake through LDHA-AKT-GLUT1 signaling has been reported in lung adenocarcinoma.[24] Based on these reports, our findings showing overexpression of PKM2 and LDHA and the correlation between degree of expression and tumor risk grade in GISTs indicate that overexpression of PKM2 and LDHA may play important roles in GIST tumorigenesis and suggest their usefulness as potential therapeutic targets.

V. CONCLUSION

In conclusion, we evaluated the usefulness of preoperative ^{18}F-FDG PET/CT for the prediction of malignant potential in GISTs and the relationship between tumor risk grade and the expression of proteins involved in glucose metabolism. Our results showed that ^{18}F-FDG uptake correlates with tumor risk grade and expression levels of GLUT1, HK1, and LDHA. The increased expression of GLUT1, HK1, PKM2, and LDHA with higher tumor risk grades indicates important roles for these proteins in GIST tumorigenesis and suggests their usefulness in the preoperative prediction of malignant potential.

REFERENCES

1. Miettinen M, Lasota J. Gastrointestinal stromal tumors: review on morphology, molecular pathology, prognosis, and differential diagnosis. Arch Pathol Lab Med 2006;130:1466-78.
2. Miller TR, Pinkus E, Dehdashti F, Grigsby PW. Improved prognostic value of 18F-FDG PET using a simple visual analysis of tumor characteristics in patients with cervical cancer. J Nucl Med 2003;44:192-7.
3. de Geus-Oei LF, Vriens D, van Laarhoven HW, van der Graaf WT, Oyen WJ. Monitoring and predicting response to therapy with 18F-FDG PET in colorectal cancer: a systematic review. J Nucl Med 2009;50 Suppl 1:43S-54S.
4. Tagliabue L, Del Sole A. Appropriate use of positron emission tomography with [(18)F]fluorodeoxyglucose for staging of oncology patients. Eur J Intern Med 2014;25:6-11.
5. Shreve P, Faasse T. Role of positron emission tomography-computed tomography in pulmonary neoplasms. Radiol Clin North Am 2013;51:767-79.
6. Gallamini A, Borra A. Role of PET in lymphoma. Curr Treat Options Oncol 2014;15:248-61.
7. Kamiyama Y, Aihara R, Nakabayashi T, Mochiki E, Asao T, Kuwano H, et al. 18F-fluorodeoxyglucose positron emission tomography: useful technique for predicting malignant potential of gastrointestinal stromal tumors. World J Surg 2005;29:1429-35.

8. Yoshikawa K, Shimada M, Kurita N, Sato H, Iwata T, Morimoto S, et al. Efficacy of PET-CT for predicting the malignant potential of gastrointestinal stromal tumors. Surg Today 2013;43:1162-7.
9. Otomi Y, Otsuka H, Morita N, Terazawa K, Furutani K, Harada M, et al. Relationship between FDG uptake and the pathological risk category in gastrointestinal stromal tumors. J Med Invest 2010;57:270-4.
10. Park JW, Cho CH, Jeong DS, Chae HD. Role of F-fluoro-2-deoxyglucose Positron Emission Tomography in Gastric GIST: Predicting Malignant Potential Pre-operatively. J Gastric Cancer 2011;11:173-9.
11. Prior JO, Montemurro M, Orcurto MV, Michielin O, Luthi F, Benhattar J, et al. Early prediction of response to sunitinib after imatinib failure by 18F-fluorodeoxyglucose positron emission tomography in patients with gastrointestinal stromal tumor. J Clin Oncol 2009;27:439-45.
12. Gayed I, Vu T, Iyer R, Johnson M, Macapinlac H, Swanston N, et al. The role of 18F-FDG PET in staging and early prediction of response to therapy of recurrent gastrointestinal stromal tumors. J Nucl Med 2004;45:17-21.
13. de Geus-Oei LF, van Krieken JH, Aliredjo RP, Krabbe PF, Frielink C, Verhagen AF, et al. Biological correlates of FDG uptake in non-small cell lung cancer. Lung Cancer 2007;55:79-87.
14. Chung JK, Lee YJ, Kim SK, Jeong JM, Lee DS, Lee MC. Comparison of [18F]fluorodeoxyglucose uptake with glucose transporter-1 expression and proliferation rate in human glioma and non-small-cell lung cancer. Nucl Med Commun 2004;25:11-7.

15. Brown RS, Goodman TM, Zasadny KR, Greenson JK, Wahl RL. Expression of hexokinase II and Glut-1 in untreated human breast cancer. Nucl Med Biol 2002;29:443-53.
16. Warburg O. On the origin of cancer cells. Science 1956;123:309-14.
17. Kim JW, Dang CV. Cancer's molecular sweet tooth and the Warburg effect. Cancer Res 2006;66:8927-30.
18. Marín-Hernández A, Gallardo-Pérez JC, Ralph SJ, Rodríguez-Enríquez S, Moreno-Sánchez R. HIF-1alpha modulates energy metabolism in cancer cells by inducing over-expression of specific glycolytic isoforms. Mini Rev Med Chem 2009;9:1084-101.
19. Miller DM, Thomas SD, Islam A, Muench D, Sedoris K. c-Myc and cancer metabolism. Clin Cancer Res 2012;18:5546-53.
20. Archer MC. Role of sp transcription factors in the regulation of cancer cell metabolism. Genes Cancer 2011;2:712-9.
21. Takebayashi R, Izuishi K, Yamamoto Y, Kameyama R, Mori H, Masaki T, et al. [18F]Fluorodeoxyglucose accumulation as a biological marker of hypoxic status but not glucose transport ability in gastric cancer. J Exp Clin Cancer Res 2013;32:34.
22. Fletcher CD, Berman JJ, Corless C, Gorstein F, Lasota J, Longley BJ, et al. Diagnosis of gastrointestinal stromal tumors: A consensus approach. Hum Pathol 2002;33:459-65.
23. Tian M, Zhang H, Nakasone Y, Mogi K, Endo K. Expression of Glut-1 and Glut-3 in untreated oral squamous cell carcinoma compared with FDG accumulation in a PET study. Eur J Nucl Med Mol Imaging 2004;31:5-12.

24. Zhou X, Chen R, Xie W, Ni Y, Liu J, Huang G. Relationship Between 18F-FDG Accumulation and Lactate Dehydrogenase A Expression in Lung Adenocarcinomas. J Nucl Med 2014;55:1766-71.
25. Park SG, Lee JH, Lee WA, Han KM. Biologic correlation between glucose transporters, hexokinase-II, Ki-67 and FDG uptake in malignant melanoma. Nucl Med Biol 2012;39:1167-72.
26. Paudyal B, Paudyal P, Oriuchi N, Tsushima Y, Nakajima T, Endo K. Clinical implication of glucose transport and metabolism evaluated by 18F-FDG PET in hepatocellular carcinoma. Int J Oncol 2008;33:1047-54.
27. Shim HK, Lee WW, Park SY, Kim H, So Y, Kim SE. Expressions of glucose transporter Types 1 and 3 and hexokinase-II in diffuse large B-cell lymphoma and other B-cell non-Hodgkin's lymphomas. Nucl Med Biol 2009;36:191-7.
28. Tanaka M, Kataoka H, Yano S, Ohi H, Moriwaki K, Akashi H, et al. Antitumor effects in gastrointestinal stromal tumors using photodynamic therapy with a novel glucose-conjugated chlorin. Mol Cancer Ther 2014;13:767-75.
29. Wong N, De Melo J, Tang D. PKM2, a Central Point of Regulation in Cancer Metabolism. Int J Cell Biol 2013;2013:242513.
30. Zhou CF, Li XB, Sun H, Zhang B, Han YS, Jiang Y, et al. Pyruvate kinase type M2 is upregulated in colorectal cancer and promotes proliferation and migration of colon cancer cells. IUBMB Life 2012;64:775-82.
31. Rong Y, Wu W, Ni X, Kuang T, Jin D, Wang D, et al. Lactate

dehydrogenase A is overexpressed in pancreatic cancer and promotes the growth of pancreatic cancer cells. Tumour Biol 2013;34:1523-30.

32. Sheng SL, Liu JJ, Dai YH, Sun XG, Xiong XP, Huang G. Knockdown of lactate dehydrogenase A suppresses tumor growth and metastasis of human hepatocellular carcinoma. FEBS J 2012;279:3898-910.

33. Miao P, Sheng S, Sun X, Liu J, Huang G. Lactate dehydrogenase A in cancer: a promising target for diagnosis and therapy. IUBMB Life 2013;65:904-10.

34. Fantin VR, St-Pierre J, Leder P. Attenuation of LDH-A expression uncovers a link between glycolysis, mitochondrial physiology, and tumor maintenance. Cancer Cell 2006;9:425-34.

35. Le A, Cooper CR, Gouw AM, Dinavahi R, Maitra A, Deck LM, et al. Inhibition of lactate dehydrogenase A induces oxidative stress and inhibits tumor progression. Proc Natl Acad Sci U S A 2010;107:2037-42.

ABSTRACT (IN KOREAN)

위장관기질종양에서 ^{18}F-fluorodeoxyglucose 섭취에 관여하는 당 대사 관련 유전자 발현 및 분자생물학적 특징

<지도교수 김 호 근>

연세대학교 대학원 의과학과

조 민 희

위장관기질종양은 중간엽 세포에서 발생된 육종으로, 주로 위장관계의 벽의 점막하 조직에 존재한다. 이렇기 때문에 수술을 하기 전에는 병기의 결정 및 악성도를 평가하기에 한계점이 존재한다.

^{18}F-fluorodeoxyglucose (^{18}F-FDG) 를 이용한 양전자방출단층촬영(positron emission tomography-computed tomography, PET/CT)은 위장관기질종양의 수술 전 진단, 예후 예측에 유용한 영상학적 기법으로 쓰이고 있다. PET/CT는 종양이 정상 조직과 달리 비정상적인 증식을 위해 당 섭취를 증가시킨다는 것에 원리를 두고 있다. 그러나,

위장관기질종양에서 ^{18}F-FDG 섭취, 즉 포도당 대사에 어떠한 분자들이 관여하는지에 대한 연구는 잘 알려지지 않았다. ^{18}F-FDG PET/CT의 판독은 표준 섭취 계수(standardized uptake value, SUV)의 측정으로 당 대사 정도를 평가하여 양성 종양과 악성 종양을 구분하고 있다.

본 연구에서는 위장관기질종양의 전반적인 당 대사를 이해하고자, PET/CT를 통하여 40명의 위장관기질종양 환자에 대한 ^{18}F-FDG 섭취를 평가하였고, 40명의 환자에 해당하는 조직을 절제하여 qRT-PCR, western blotting, immunohistochemistry를 통해 당 분해 효소들의 발현을 분석하였다.

ROC (receiver operating characteristic) curve 분석을 통하여 high-risk 종양 (악성)을 구분하기 위한 최대표준섭취계수의 cut-off 값을 4.99로 좁혔다 (sensitivity, 89.5%; specificity, 76.2%; accuracy, 82.5%). 또한 당 분해과정에 관여하는 GLUT1, HK1, LDHA의 발현 정도와, 최대표준섭취계수가 양의 상관관계를 보이는 것을 확인하였다. 특히, 위장관기질종양의 high-risk 조직에서 GLUT1, HK1, PKM2, LDHA의 과발현을 확인하였다.

따라서 이러한 결과들은 GLUT1, HK1, PKM2, LDHA의 upregulation이 위장관기질종양 형성 과정에 중요한 역할을 하며, 수술 전 위장관

기질종양의 악성도 예측 지표로 유용하게 활용될 수 있을 것이라 기대한다.

핵심되는 말: 위장관 기질종양, 최대표준섭취계수, 악성도, 당 대사

PUBLICATION LIST

1. Cho MH, Park CK, Park M, Kim WK, Cho A, Kim H. Clinicopathologic Features and Molecular Characteristics of Glucose Metabolism Contributing to ^{18}F-fluorodeoxyglucose Uptake in Gastrointestinal Stromal Tumors. PLoS One 2015;10:e0141413.